applied sciences

MDPI

Article

Optimization of ER8 and 42CrMo4 Steel Rail Wheel for Road–Rail Vehicles

Filip Lisowski [1,*] and Edward Lisowski [2]

1 Institute of Machine Design, Cracow University of Technology, ul. Warszawska 24, 31-155 Cracow, Poland
2 Institute of Applied Informatics, Cracow University of Technology, ul. Warszawska 24, 31-155 Cracow, Poland; edward.lisowski@pk.edu.pl
* Correspondence: filip.lisowski@pk.edu.pl

Received: 1 June 2020; Accepted: 5 July 2020; Published: 8 July 2020

check for updates

Abstract: Railway track maintenance services aim to shorten the time of removing failures on the railways. One of the most important element that shorten the repair time is the quick access to the failure site with an appropriate equipment. The use of road-rail vehicles is becoming increasingly important in this field. In this type of constructions, it is possible to use proven road vehicles such as self-propelled machines or trucks running on wheels with tires. Equipping these vehicles with a parallel rail drive system allows for quick access to the failure site using both roads and railways. Steel rail wheels of road-rail vehicles are designed for specific applications. Since the total weight of vehicle is a crucial parameter for roadworthiness, the effort is made to minimize the mass of rail wheels. The wheel under consideration is mounted directly on the hydraulic motor. This method of assembly is structurally convenient, as no shafts or intermediate couplings are required. On the other hand, it results in strict requirements for the wheel geometry and can cause significant stress concentration. Therefore, the problem of wheel geometry optimization is discussed. Consideration is given to the use of ER8 steel for railway application and 42CrMo4 high-strength steel. Finite element analysis within Ansys software and various optimization tools and methods, such as random tool, subproblem approximation method and first-order method are applied. The obtained results allow to minimize the rail wheel mass with respect to the used material. Moreover, computational demands and methods leading to the best results are compared.

Keywords: rail wheel; rail-road vehicle; parametric optimization; finite element analysis

1. Introduction

Road-rail vehicles are designed to operate on both roads and tracks. Running on rails is carried out by means of a rail drive system. Such a system can be used for driving the vehicle on the track or as a power unit. In the first case, the vehicle's tires run on rails and the rail wheels only guide the vehicle on the track. In the second case, the vehicle is raised above the rail head level and the rail unit has an independent drive. The drivetrain unit can be equipped with a friction drive system or hydraulic motors [1,2]. The use of large diameter rail wheels in these vehicles would significantly increase the curb weight of the truck. However, when the vehicle covers most of the route on the road, the route covered on the track is shorter. Therefore, driving at speed up to 50 km/h is sufficient. Consequently, it is possible to equip these vehicles with smaller diameter rail wheels, which do not significantly increase the curb weight of the truck. Rail wheels for road-rail vehicles are designed for a specific application depending on the required strength and function. It is advisable to optimize the structure in order to minimize the wheel mass, while providing sufficiently high mechanical strength. Problems related to the optimization of the rail wheels for rolling stock were considered by authors of several publications. (Nielsen and Fredö, 2006) [3] presented a numerical procedure of multi-disciplinary optimization of railway wheels. Fatigue strength, mass minimization and rolling noise were considered. Self-adaptive genetic optimization algorithms were applied to solve the problem. In the study [4], (Choi et al., 2013) presented the problem of multi-objective optimization of wheel profile to minimize both flange wear and surface fatigue. The optimization was carried out using a genetic algorithm. Whereas the problem concerning optimization of both the geometry of wheel and rail profile in order to improve tractive and braking forces was discussed in the study [5] (Liu et al., 2016). (Ignesti et al., 2014) [6] developed an innovative new rail wheel profile optimized to improve wear and stability. The study on optimization of the rail profile for heavy haul railways was presented by (Wang et al., 2016) in the paper [7]. An innovative method for reverse design of rail wheel profiles was presented in study by (Chen et al. 2018) [8]. The method was based on mapping the differences in the rolling radius and allowed to reduce the stress in contact between the wheel and the rail. (Bracciali et al., 2019) [9] presented the study on a tired rail wheel with the web made of austempered ductile iron including casting simulation as well as static and fatigue strength assessment. The wheel was designed to operate in a diesel multiple unit. Whereas a numerical evaluation of the fatigue load capacity of the cylindrical crane wheel was presented by (Romanowicz, 2017) in the article [10]. The application of multiaxial high-cycle fatigue criteria for the analysis of the subsurface rolling contact fatigue of structures working in contact conditions was discussed. The multiaxial fatigue analysis is applied when the equivalent fatigue stress for complex loading is investigated.

In turn, various examples of applying the finite element numerical analysis in optimal design of structures were presented in works [11–17], and those using Ansys software in papers [18–21].

Nevertheless, all of the studies on rail wheels mentioned above concerned the use for railcars and locomotives, but not for road-rail vehicles as referred to in herein. This article concerns the problem of a monobloc rail wheel optimization dedicated for the rail-road vehicle shown in Figure 1. The main goal is to minimize the mass of the wheel depending on used material and obtain the required fatigue strength. The analysis is conducted using Ansys Mechanical APDL software (Release 18.2, ANSYS Europe, Ltd.).

Figure 1. Road-rail vehicle with hydraulic driven rail system.

2. Rail Wheel Materials

The most commonly used materials for monobloc wheels and rims for rolling stock in Europe are carbon steels with a carbon content not exceeding 0.56% [22]. Fine grain, high purity and high homogeneity are required around the entire wheel circumference. Steels used on wheels for a rolling stock should have mainly a perlite structure containing hard cementite lamellas to provide wear resistance. A ferrite content of less than 10% is advantageous in order to minimize rim wear. The wheel material is subjected to thermal treatment, which improves its mechanical properties and resistance to abrasive wear. EN 13262 [23] standard specifies four steel grades for monoblock wheels, which are ER6, ER7, ER8 and ER9. The above steel grades differ in their chemical composition and consequently in their mechanical strength. Most often the ER7 grade is used in freight and passenger wagons. Whereas, ER8 grade is used for driving wheels in locomotives and drivetrain units. Therefore, the first material accepted for further analysis is ER8 steel.

The second material adopted for consideration is 42CrMo4 high grade molybdenum alloy steel defined in EN 10083 standard [24]. This low-alloy steel is widely used for highly loaded components of driving units. It is used for drive shafts, gears, bearing raceways, but also for crane rail wheels. The material is intended for heat treatment and is well suitable for cold forging [25]. Molybdenum content significantly improves mechanical properties in the tempered condition. The resistance to wear can be considerably increased by flame hardening or nitriding. The chemical composition of accepted steels is specified in Table 1, whereas the mechanical properties are summarized in Table 2.

Table 1. Chemical composition of ER8 and 42CrMo4 steels.

	Maximum Content in%										
Steel grade	C	Si	Mn	P	S	Cr	Cu	Mo	Ni	V	Cr + Mo + Ni
ER8	0.56	0.40	0.80	0.020	0.015	0.30	0.30	0.08	0.30	0.06	0.50
42CrMo4	0.45	0.40	0.09	0.025	0.035	1.2	–	0.30	–	–	–

Table 2. Mechanical properties of ER8 and 42CrMo4 steels.

Steel Grade	Yield Strength Re (MPa)	Tensile Strength Rm (MPa)	Elongation A (%)
ER8	min. 540	860–980	min. 13
42CrMo4	min. 900	1100–1300	min. 10

3. Rail Wheel Design

The rail wheel under consideration is mounted directly on the hydraulic motor with drum brake. The wheel is cantered and fixed by means of ten thread-in wheel studs and cone nuts as shown in Figure 2. A tightening torque is 300 Nm. The axial tensile force per single stud of about 26 kN is obtained by taking the nut cone angle of 60° and friction coefficient of 0.5 [26].

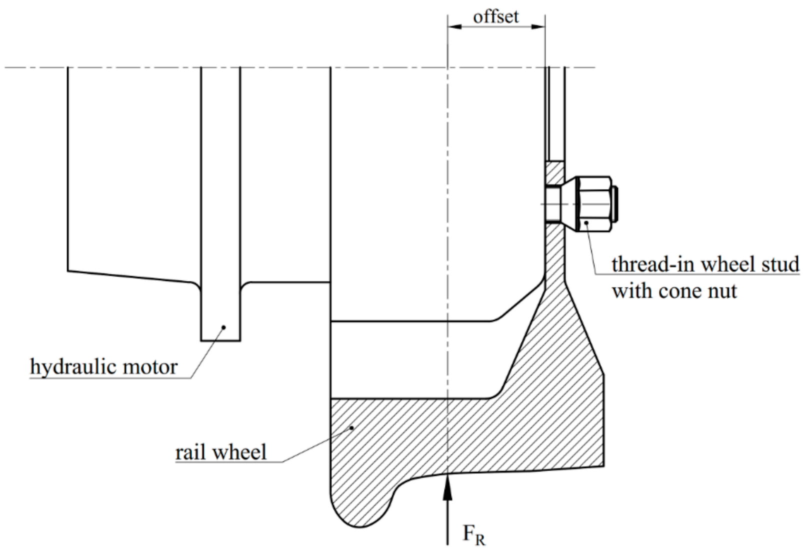

Figure 2. Assembly of rail wheel on hydraulic motor with drum brake.

The offset from shaft end face is the main parameter limiting the radial load and thus the position of a wheel web. The permitted radial load of accepted hydraulic motor is shown in Figure 3. While analyzing the graph, it can be noticed that higher values of permissible radial load are obtained for negative offset values. The maximum radial force is achieved for the offset equal to 35 mm below zero.

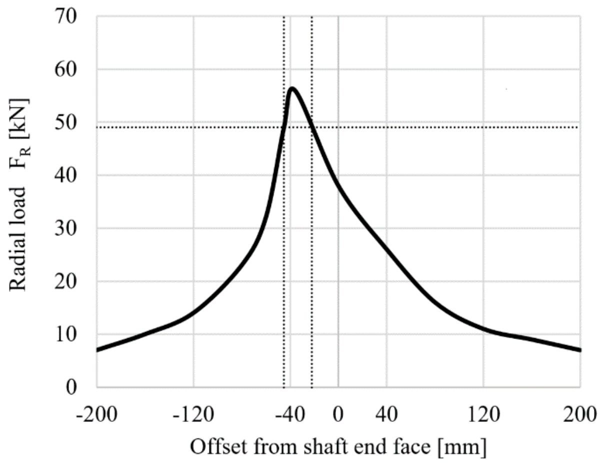

Figure 3. Permitted radial load of hydraulic motor drive shaft. (Dotted lines refer to the permitted radial load and offset range for maximum vehicle mass).

The maximum vehicle mass of 32,000 kg is assumed to be distributed evenly over eight rail wheels. The radial load per one wheel is therefore 4000 kg, which corresponds to a force of 39.24 kN. However, taking into account a dynamic factor of 1.25, the permitted radial load of 49.05 kN is obtained. The value of dynamic load factor is taken depending on the type of component and the corresponding standard [27]. Thus, the acceptable offset range is between 22 and 45 mm below zero. The fatigue strength of monobloc rail wheels must be checked in accordance with EN 13979 standard [27]. For wheels with machined wheel web, the range of the dynamic stress $\Delta\sigma = \sigma_{max} - \sigma_{min}$ must be less than 360 MPa within all nodes, where σ_{max} is the maximum principal stress and σ_{min} is the minimum stress equal to the lowest normal stress in the direction of σ_{max}.

4. Optimization Problem

The aim of the optimization problem is to minimize the mass of the rail wheel for road-rail vehicle under specified constrains of design and state variables. ER8 and 42CrMo4 steel grades are considered for the wheel material. The geometric limitations are mainly due to the space for the hydraulic motor and permitted offset from the hydraulic motor shaft end face. Whereas, the stress limits are related to the permissible dynamic stress and yield strength. The optimization problem is performed through the finite element analysis using Ansys software. In addition, various optimization tools and methods are used to achieve the best solution.

4.1. Finite Element Model

Three dimensional parametric model of rail wheel is prepared in order to solve optimization problem. The model is fixed and loaded as shown in Figure 4. The 20-node SOLID186 finite elements are used to generate mesh within volumes. CONTA174 and TARGET170 elements are used to define contact between the fixed points and cylindrical surfaces of holes in the wheel web. A symmetry constrain on the wheel surface is set since half of the wheel geometry is considered. Displacements of the inner surface of wheel web are locked in the x direction. Radial load F_R and pressure representing bolt pretension are applied. It is identified that the maximum principal stress σ_{max} occurs at the edge of the upper or lower bolt hole, and the maximum stress amplitude $\Delta\sigma$ is achieved when the wheel is rotated by 180°. Therefore, in order to calculate the stress amplitude exactly in the same nodes of mesh, two load steps with radial load applied on opposite sides of the rim are defined. Lateral loads are not included in the analysis under the assumption that the speed of the vehicle on the track is relatively low and the vehicle runs on short sections of straight tracks between level crossings. Furthermore, there are no axles between the wheels in the rail drive system of the analyzed road-rail vehicle. Each wheel is driven separately by an independent hydraulic motor, which eliminates slippage and reduces lateral forces. The use of independent wheel drive and a conical wheel profile results in continuous centering of the vehicle in the track. For the nominal wheel position on the rail, the cone angle of the wheel profile is very small. The resulting lateral force due to the conicity of the wheel is therefore negligible compared to the vertical forces.

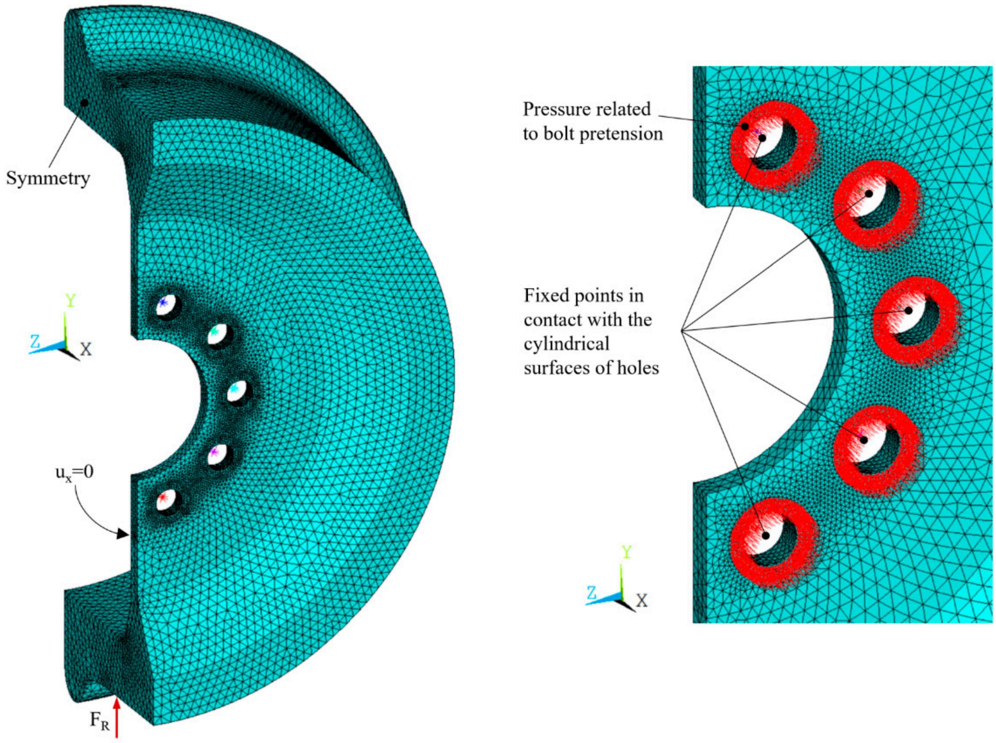

(**a**) (**b**)

Figure 4. Finite element model of rail wheel with boundary conditions and loads. (**a**) View of the entire model; (**b**) view of bolt holes.

Mesh Validation

When the finite element analysis is used to determine stresses, the mesh validation should be conducted. Convergence of the results should arise from the mesh refinement [27]. The parameter having critical influence on the results is the mesh size within the influence zone, which is accepted around bolt holes. The convergence of the results is verified concerning maximum von Mises stress in the function of element numbers as shown in Figure 5. The minimum number of finite elements to be accepted in the influence zone is about 68,900.

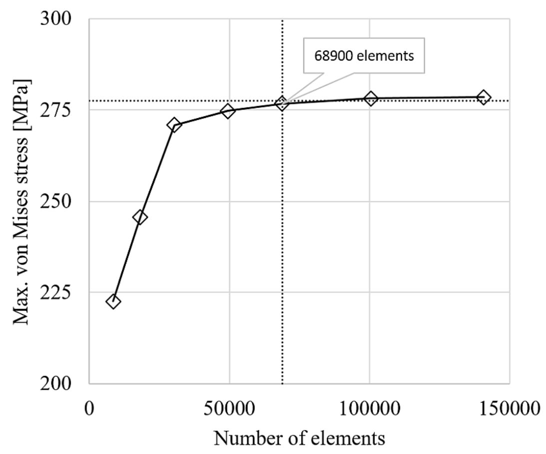

Figure 5. Maximum von Mises stress depending on the finite elements number in the influence zone.

4.2. Design and State Variables

The geometry of the rail wheel section is parameterized as shown in Figure 6. The dimensions which are not subjected to modification are related to the rim profile, wheel web thickness and rolling diameter. The dimension of 70 mm is the lateral radial load distance from the inner face of the wheel. The value of exactly 70 mm is specified in standard EN 13979-1: 2003 + A2: 2011. It corresponds to the 'Case 1', which is the operation on a straight track under the assumption that the wheel set is centered.

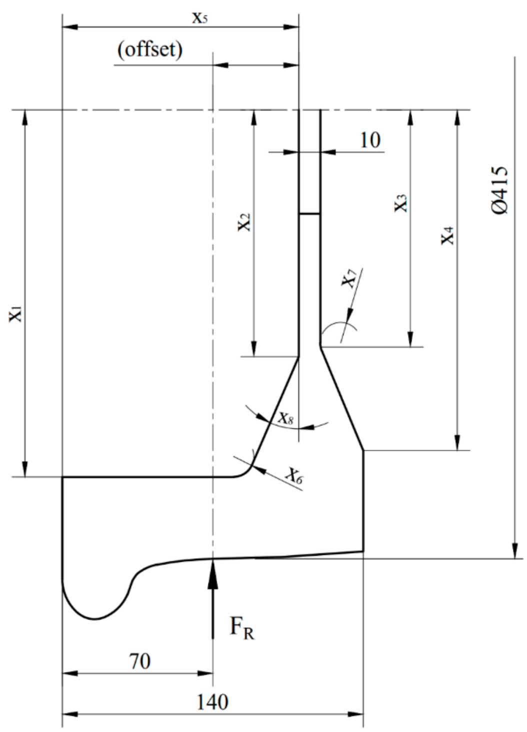

Figure 6. Rail wheel profile geometry with main dimensions (in mm) and design variables.

Variables $x1 - x4$ are the radii of the wheel section, $x5$ is the distance between the rim face and wheel web, $x6 - x7$ are the rounding radii and $x8$ is the slope angle of the inner surface of the wheel web. Design variables and their constrains are summarized in Table 3, while state variables with constrains are specified in Table 4. The constraints of state variables result from the strength requirements. Apart from the condition for dynamic stress $\Delta\sigma < 360$, it was assumed that the safety factor related to yield stress must be at least 2.0.

Table 3. Design variables (in mm).

Design Variables	x1	x2	x3	x4	x5	x6	x7	x8
Constrains	145< <175	110< <135	105< <175	105< <175	92< <105	5< <10	5< <10	1°< <20°

Table 4. State variables.

State Variables	Dynamic Stress $\Delta\sigma$ [MPa]	Safety Factor k = max (σ_{vm})/Re *
Constrains	<360	≥2.0

* max (σ_{vm}) is the maximum von Mises stress.

4.3. Optimization Methods

Several optimization tools and methods are available within Ansys Mechanical APDL design optimization module. Optimization tools are used to measure and understand the design space of the problem, whereas optimization methods are techniques used to minimize a single objective function subjected to constraints. The available tools are: random, gradient, sweep, factorial and single loop analysis tool. Above tools can be used for initial investigation in order to determine convenient starting point or to obtain the number of random results as a precursor for further subproblem optimization. Related details of all tools are described in Ansys Release guide [28]. The available optimization methods are: subproblem approximation method and first-order method. The random tool and both of optimization methods mentioned above are applied within the optimization problem described in this study.

4.3.1. Random Tool

The random tool generates random values of a variable vector $\boldsymbol{x}$ for each iteration as given by Equation (1). There is no need to define objective functions and state variables. However, it can be useful if the actual optimization is carried out subsequently [29].

$$\boldsymbol{x} = \boldsymbol{x}^* = randomly\ generated\ vector \tag{1}$$

4.3.2. Subproblem Approximation Method

The subproblem approximation method is described as an advanced zero-order iteration method, which requires the values of the dependent variables but not their derivatives [29]. As this method is based on approximation of the objective function and all state variables, a certain number of design sets is required. This initial data can be generated by user using one of the available optimization tool. Otherwise they are generated randomly by program. Dependent variables like objective function and state variables are approximated by means of last square fitting. The objective function is in a quadratic form as given by Equation (2):

$$\hat{f} = a + \sum_{i}^{n} b_i \boldsymbol{x}_i + \sum_{i}^{n} c_i \boldsymbol{x}_i^2 + \sum_{i}^{n} \sum_{j}^{n} d_{ij} \boldsymbol{x}_i \boldsymbol{x}_j \tag{2}$$

where $\hat{f}$ is approximated objective function, a, b, c and d are weighted coefficients of last squares technique, $\boldsymbol{x}$ represents design variables vector, n is the number of iterations, i stays for the variable number and j is number of loops. In the next step, a constrain problem is transform to an unconstrained problem by means of the penalty functions. The obtained objective function that is minimize is given by Equation (3):

$$Q(\boldsymbol{x},\ p_k) = \hat{f} + f_0 p_k \left(\sum_i^n X(\boldsymbol{x}_i) + \sum_i^{m_1} G(\hat{g}_i) + \sum_i^{m_2} H\left(\hat{h}_i\right) + \sum_i^{m_3} W(\hat{w}_i) \right) \quad (3)$$

where X is the penalty function for design variable constrains, G, H and W are penalty functions referred to state variables, f_0 is the reference objective function and p_k is penalty parameter.

4.3.3. First Order Method

The first-order method in contrast to the subproblem approximation method uses derivatives formed for the objective function and state variable penalty functions. A direction in design space is searched by means of step descent method and conjugate gradient method. In each iteration a number of substeps are performed in order to calculate direction and gradient. In comparison to previous method, the first-order method is usually perceived as more accurate and at the same time more computationally demanding [28]. An unconstrained form of the objective function is formulated as given by Equation (4):

$$Q(\boldsymbol{x},\ q) = \frac{f}{f_0} + \sum_i^n P_{\boldsymbol{x}}(\boldsymbol{x}_i) \left(\sum_i^{m_1} P_g(g_i) + \sum_i^{m_2} P_h(h_i) + \sum_i^{m_3} P_w(w_i) \right) \quad (4)$$

where P_x, P_g and P_w are the penalty functions referred to the constrained design and state variables, f_0 is the reference objective function and p_k is penalty parameter, q is the surface response parameter that controls the satisfaction of the constraint.

4.4. Results and Discussion

The results of optimization were obtained by the use of random tool, subproblem approximation method and first-order method with various settings. The variants accepted for the comparison are summarized in Table 5. The best results of the minimized objective function, which was the rail wheel mass, are presented in Figure 7. The number of iteration loops to obtain the feasible solution is shown in Figure 8. Concerning the use of ER8 steel, the best optimization result was obtained applying first-order method with the resulted rail wheel mass of 38.1 kg. In turn, for the use of subproblem approximation method the obtained mass was 0.5%–5.5% higher. However, the number of iteration loops was significantly lower. Regarding to the use of 42CrMo4 steel, the best optimization result was achieved applying subproblem approximation method preceded by the use of random tool with 15 iterations. The resulting rail wheel mass of 33.9 kg was obtained.

Table 5. Optimization methods variants.

R5 + Sub	subproblem approximation method preceded by the use of random tool with 5 iterations
R15 + Sub	subproblem approximation method preceded by the use of random tool with 15 iterations
R30 + Sub	subproblem approximation method preceded by the use of random tool with 30 iterations
First	first-order method with an initial point at the upper limit of the design variables

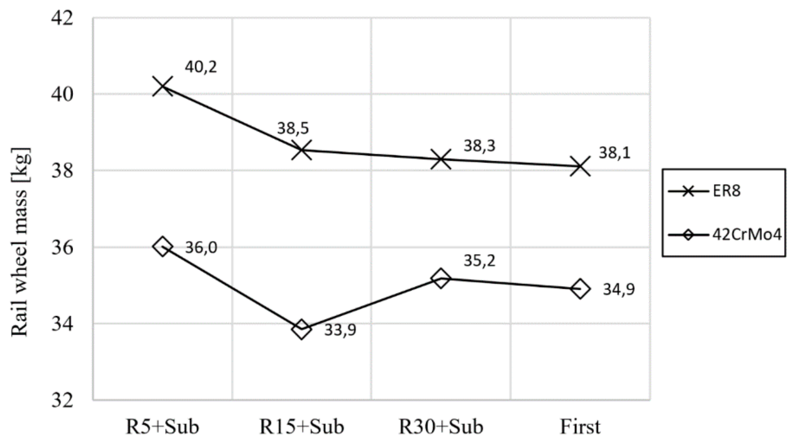

Figure 7. Optimized rail wheel mass for various variants of optimization method.

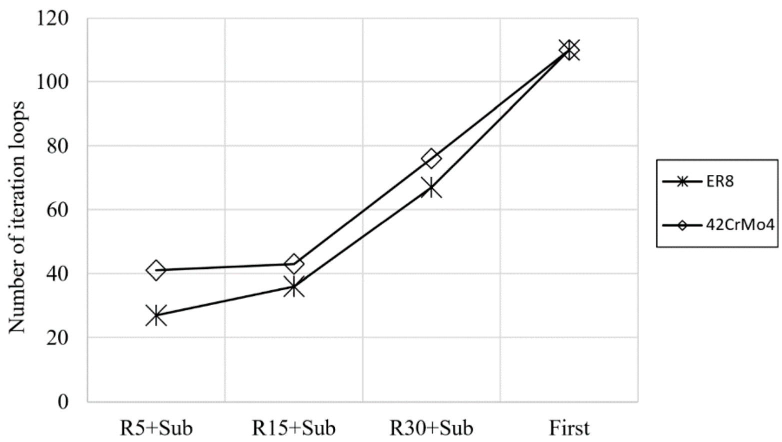

Figure 8. Number of iteration loops for various variants of optimization method.

Concerning the optimization using the subproblem approximation method, it was expected that increasing the initial number of random results should lead to a better solution. However, as it could be noticed for optimization of wheel made of 42CrMo4 steel, such a consequence did not occur. Instead, the mass obtained for the optimization case R30 + Sub was higher than for the case R15 + Sub, which requires an explanation. This could be caused by insufficient number of feasible initial data or by an objective function tolerance that affected the termination of calculations. During the optimization process, the first approximation of objective function was made on the basis of initial random set generated and the next approximations also included results of optimization iterations. However, due to strict constrains on the independent state variables, all initial random results were infeasible (the restrictions on state variables were not met) mainly due to constraints on $\Delta\sigma$. For all reported cases, the same software default solution convergence criteria were accepted. The convergence of the solution was obtained when two consecutive results were feasible and the difference in the value of the objective function was less than accepted tolerance equal to 0.01 of the current set. Further investigations—including the impact of the feasible initial results number and the range of objective function tolerance that terminates calculations—should be developed to indicate the relevant cause of the lack of result improvement for the case of R30 + Sub.

The optimal geometry of rail wheel profile is shown in Figure 9, whereas design and state variables were summarized in Tables 6 and 7. Comparing the best optimization results for both considered materials, the mass of rail wheel made of 42CrMo4 steel was over 11% lower.

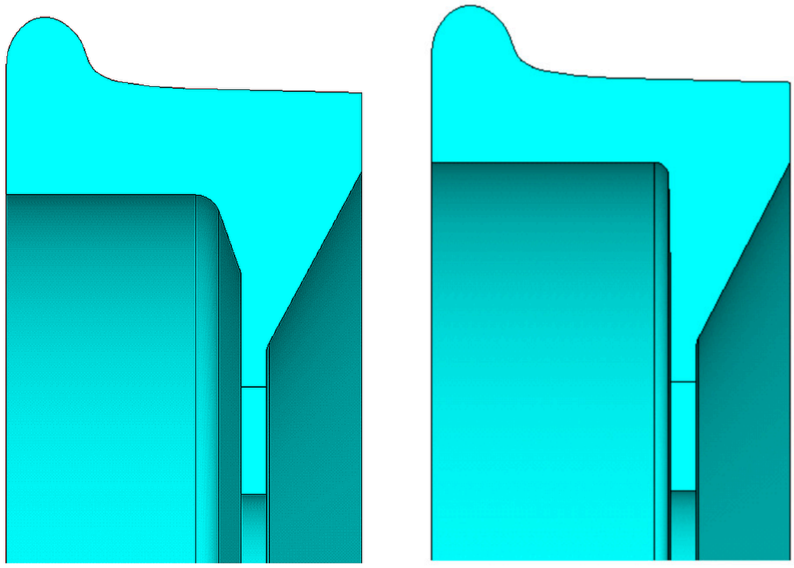

(a) (b)

Figure 9. Optimal geometry of rail wheel profile made of steel: (**a**) ER8, mass: 38.1 kg; (**b**) 42CrMo4, mass: 33.9 kg.

Table 6. Design variables (in mm) for best optimization result.

Design Variables	*x1*	*x2*	*x3*	*x4*	*x5*	*x6*	*x7*	*x8*
ER8	165.6	134.9	105.4	175.0	92.3	9.9	9.9	19.5°
42CrMo4	174.9	124.8	105.3	174.9	93.4	5.6	7.4	1.1°

Table 7. State variables for best optimization result.

State Variables	Dynamic Stress Δσ [MPa]	Safety Factor k
ER8	249	2.0
42CrMo4	358	3.2

Figures 10 and 11 show the von Mises stress distribution and maximum principal stress distribution for the optimal rail wheel geometry made of 42CrMo4 steel, which was the best result of the entire analysis. The greatest stress concentration of von Mises reduced stress occurs at the edge of the bottom bolt hole (Figure 10b). However, the safety factor related to the yield strength was $k = 3.2$. Therefore, no plastic deformation occurred. In turn, the highest value of the maximum principal stress occurred above the upper bolt hole (Figure 11b). The wheel web material was compressed by the bolt pretension around the hole. Deformation of the wheel under the radial load caused significant tensile stress on the boundary of this zone. When the wheel rolls, the highest dynamic stress $\Delta\sigma$ that could cause fatigue failure occurs just in that particular location.

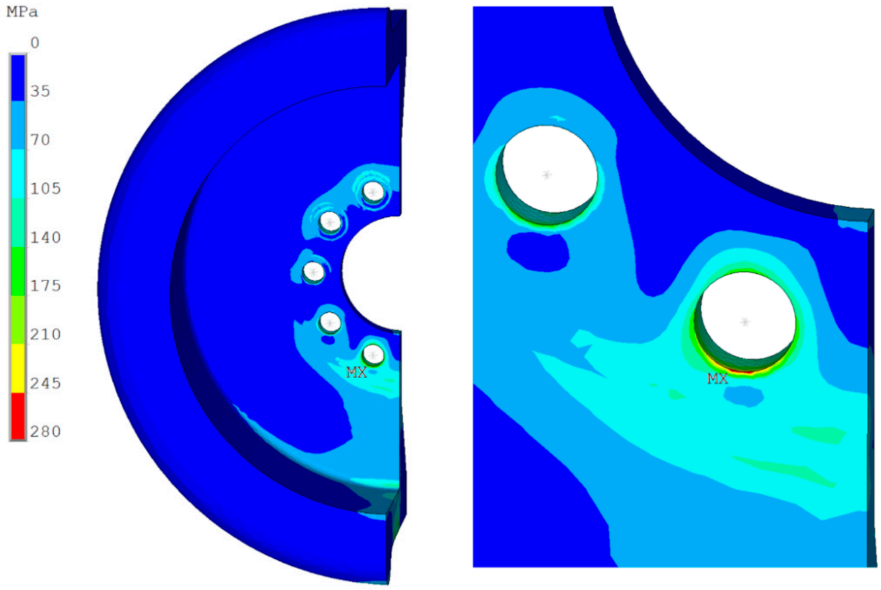

(**a**) (**b**)

Figure 10. Von Mises stress distribution for the optimal rail wheel geometry made of 42CrMo4 steel. (**a**) View of the entire model; (**b**) view of the stress concentration point.

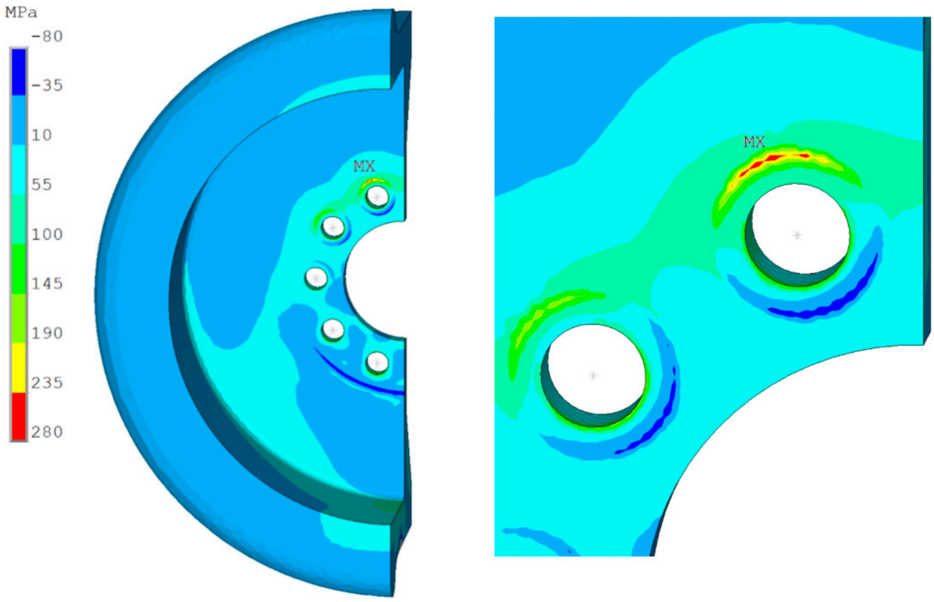

(**a**) (**b**)

Figure 11. Maximum principal stress distribution for the optimal rail wheel geometry made of 42CrMo4 steel. (**a**) View of the entire model; (**b**) view of the stress concentration point.

5. Conclusions

A study on the rail wheel for road-rail vehicle was carried out in order to minimize the mass depending on applied material. The use of ER8 and 42CrMo4 steel grades was considered. An analysis of the wheel installation on the hydraulic motor with drum brake was carried out in order to select the permitted range of the radial load offset. Finite element analysis including mesh validation was used to conduct the optimization problem. Preliminary results of finite element analysis revealed stress concentration points and highest dynamic stress location. The wheel geometry was optimized with random tool as well as subproblem approximation method and first-order method using Ansys Mechanical APDL software. Both the constraints on dynamic stress $\Delta\sigma$ (in order to avoid fatigue failure) and the constraints on maximum von Mises stress (in order to avoid plastic deformations) were defined. A safety factor of at least 2.0 was required. Results for various optimization methods and different numbers of iteration loops were compared. The best optimization result for ER8 steel was a wheel mass of 38.1 kg, with a safety factor of 2.0, while for 42CrMo4 steel the lowest obtained mass was 33.9 kg with the safety factor of 3.2. Therefore, when comparing the use of the above steel grades as the rail wheel material for road-rail vehicle, the adoption of 42CrMo4 steel allowed a mass reduction of over 11% with a safety factor higher by 38% than for ER8 steel.

Author Contributions: Conceptualization, F.L. and E.L.; methodology, F.L. and E.L.; software, E.L.; validation, F.L., writing—original draft preparation, F.L. and E.L.; visualization, F.L. All authors have read and agreed to the published version of the manuscript.

Funding: This research received no external funding.

Conflicts of Interest: The authors declare no conflicts of interest.

References

1. Medwid, M.; Jakuszko, W.; Łukaszewski, K.; Bryk, K. Rail running gear with friction-drum drive. *Pojazdy Szynowe* **2018**, *1*, 35–44.
2. Cichy, R.; Magnucka-Blandzi, M.; Nowicki, M. Durability tests of road-rail vehicles to receive operation admission. *Pojazdy Szynowe* **2018**, *1*, 45–54.
3. Nielsen, J.C.O.; Fredö, C.R. Multi-disciplinary optimization of railway wheels. *J. Sound Vib.* **2006**, *293*, 510–521. [CrossRef]
4. Choi, H.Y.; Lee, D.H.; Lee, J. Optimization of a railway wheel profile to minimize flange wear and surface fatigue. *Wear* **2013**, *300*, 225–233. [CrossRef]
5. Liu, B.; Mei, T.X.; Bruni, S. Design and optimisation of wheel–rail profiles for adhesion improvement. *Veh. Syst. Dyn.* **2016**, *54*, 429–444. [CrossRef]
6. Ignesti, M.; Innocenti, A.; Marini, L.; Meli, E.; Rindi, A. A numerical procedure for the wheel profile optimisation on railway vehicles. *Proc. IMechE Part J J. Eng. Tribol.* **2014**, *228*, 206–222. [CrossRef]
7. Wang, P.; Gao, L.; Xin, T.; Cai, X.; Xiao, H. Study on the numerical optimization of rail profiles for heavy haul railways. *Proc. Inst. Mech. Eng. Part F J. Rail Rapid Transit* **2016**. [CrossRef]
8. Chen, R.; Hu, C.; Xu, J.; Wang, P.; Chen, J.; Gao, Y. An Innovative and Efficient Method for Reverse Design of Wheel-Rail Profiles. *Appl. Sci.* **2018**, *8*, 239. [CrossRef]
9. Bracciali, A.; Masaggia, S.; Megna, G.; Veneri, E. Quiet and light spoked wheel centres made of Austempered Ductile Iron. In Proceedings of the XIX International Wheelset Congress, Venice, Italy, 16–20 June 2019.
10. Romanowicz, P. Numerical assessment of fatigue load capacity of cylindrical crane wheel using multiaxial high-cycle fatigue criteria. *Arch. Appl. Mech.* **2017**, *87*, 1707–1726. [CrossRef]
11. Jian, L.; Shi, Y.; Wei, J.; Zheng, Y.; Deng, Z. Design Optimization and Analysis of a Dual-Permanent-Magnet-Excited Machine Using Response Surface Methodology. *Energies* **2015**, *8*, 10127–10140. [CrossRef]
12. Wang, Y.; Qian, C.; Kong, L.; Zhou, Q.; Gong, J. Design Optimization for the Thin-Walled Joint Thread of a Coring Tool Used for Deep Boreholes. *Appl. Sci.* **2020**, *10*, 2669. [CrossRef]
13. Zhong, G.; Liu, P.; Mei, X.; Wang, Y.; Xu, F.; Yang, S. Design Optimization Approach of a Large-Scale Moving Framework for a Large 5-Axis Machining Center. *Appl. Sci.* **2018**, *8*, 1598. [CrossRef]
14. Wang, G.; Zhu, D.; Liu, N.; Zhao, W. Multi-Objective Topology Optimization of a Compliant Parallel Planar Mechanism under Combined Load Cases and Constraints. *Micromachines* **2017**, *8*, 279. [CrossRef]
15. Orme, M.; Madera, I.; Gschweitl, M.; Ferrari, M. Topology Optimization for Additive Manufacturing as an Enabler for Light Weight Flight Hardware. *Designs* **2018**, *2*, 51. [CrossRef]
16. Sleesongsom, S.; Bureerat, S. Topology Optimisation Using MPBILs and Multi-Grid Ground Element. *Appl. Sci.* **2018**, *8*, 271. [CrossRef]

17. Slavov, S.; Konsulova-Bakalova, M. Optimizing Weight of Housing Elements of Two-stage Reducer by Using the Topology Management Optimization Capabilities Integrated in SOLIDWORKS: A Case Study. *Machines* **2019**, *7*, 9. [CrossRef]
18. Szybiński, B.; Romanowicz, P.J. Optimization of Flat Ends in Pressure Vessels. *Materials* **2019**, *12*, 4194. [CrossRef]
19. Lisowski, F. Optimization of thread root undercut in the planetary roller screw. *Tech. Trans.* **2017**, *9*, 219–227. [CrossRef]
20. Lisowski, F. Optimization of a curvilinear thread profile in a planetary roller screw. *Tech. Trans.* **2015**, *2-M*, 149–156.
21. Lisowski, F. Application of finite element method in the optimal design of the nut with a groove in the end-face. *Tech. Trans.* **2013**, *1-M*, 237–244.
22. Railway-Research. Available online: http://railway-research.org/IMG/pdf/760.pdf (accessed on 20 May 2020).
23. European Standard. *Railway Applications. Wheelsets and Bogies—Wheels—Product Requirements*; EN 13262: 2004+A2:2011; CEN: Brussels, Belgium, 2011.
24. European Standard. *Steels for Quenching and Tempering. Technical Delivery Conditions for Alloy Steels*; EN 10083-3:2006; CEN: Brussels, Belgium, 2006.
25. Bayrak, M.; Ozturk, F.; Demirezen, M.; Evis, Z. Analysis of Tempering Treatment on Material Properties of DIN 41Cr4 and DIN 42CrMo4 Steels. *J. Mater. Eng. Perform.* **2007**, *16*, 597–600. [CrossRef]
26. The Engineering ToolBox. Available online: https://www.engineeringtoolbox.com/friction-coefficients-d_778.html (accessed on 20 May 2020).
27. European Standard. *Railway Applications. Wheelsets and Bogies. Monobloc Wheels. Technical Approval Procedure Forged and Rolled Wheels*; EN 13979-1:2003+A2:2011; CEN: Brussels, Belgium, 2011.
28. *Ansys Academic Research Mechanical, Release 13, Help System, Design Optimization*; ANSYS Europe, Ltd.
29. Fedorik, F.; Kala, J.; Haapala, A.; Malaska, M. Use of design optimization techniques in solving typical structural engineering related design optimization problems. *Struct. Eng. Mech.* **2015**, *55*, 1121–1137. [CrossRef]